Available online at www.sciencedirect.com

ScienceDirect

Ceramics International 40 (2014) 3445–3451

CERAMICS INTERNATIONAL

www.elsevier.com/locate/ceramint

A simple annealing process to obtain highly transparent and conductive indium doped tin oxide for dye-sensitized solar cells

Ian Y.Y. Bu*

Department of Microelectronics Engineering, National Kaohsiung Marine University, 81157 Nanzih District, Kaohsiung City, Taiwan, Republic of China

Received 5 August 2013; received in revised form 11 September 2013; accepted 20 September 2013
Available online 26 September 2013

Abstract

A simple annealing process is proposed to utilize indium tin oxide (ITO) coated glass substrate in dye sensitized solar cells (DSSCs). It is shown that highly transparent thin films with low sheet resistivity can be obtained by annealing amorphous-phase rich ITO. The deposited ITO films have been extensively characterized through scanning electron microscopy (SEM), X-ray diffraction (XRD), UV–vis spectroscopy and electrical measurements. DSSCs fabricated by the proposed method have achieved a conversion efficiency of up to 4.48%. It is found that, when the film's thickness exceeds the critical thickness, 500 nm, the annealing process causes adverse effects on the film's optoelectronic properties.

Keywords: Indium tin oxide; Dye sensitized solar cells; Photoanode; Annealing; Sheet resistance

1. Introduction

Ever since the successful demonstration of dye-sensitized solar cells (DSSCs) [1], there have been great efforts into improving its performances. Typical configuration of DSSCs consists of a dyed titanium dioxide (TiO_2) nanoparticle film, an electrolyte, and a catalyst layer, which are sandwiched between two pieces of transparent conductive oxide (TCO) electrodes [2]. In general, the TiO_2 coated TCO and the catalyst coated TCO are termed photoanode and counter electrode, respectively. During the fabrication of DSSCs, the photoanode is formed by sintering TiO_2/cellulose paste coated TCO at temperatures higher than 450 °C [3–5]. Currently, the most widely employed TCO in DSSCs is fluorine doped tin oxide (FTO), due to its ability to withstand the harsh sintering process without significantly reducing optical transparency and sheet resistance [6,7]. The purposes of TiO_2 sintering process are to remove residual organic compounds that are used to form TiO_2 paste; to provide the required energy in order to promote intercalation between the individual TiO_2 nanoparticles; and to create pores between TiO_2 nanoparticles in order to increase the dye absorption [8–10]. However, the main disadvantages of using FTO in DSSCs are its relatively poor transmittance and high electrical resistivity [6,11]. In fact, a recent cost analysis reveals that FTO glass constitutes around 40% of the overall material cost of the fabricated DSSCs [12].

In terms of performance, indium tin oxide (ITO) offers superior optical transmittance and lower sheet resistivity than FTO [11]. It should be emphasized that, because ITO is likely to crack under thermal annealing [19,20], it is seldom used in DSSCs. Nevertheless, ITO has been used in other types of solar cells [13,14], light emitting diodes [15,16], display industry [17], and touch panels [18]. In the past, ITO has been deposited by using sol–gel deposition [21], spray pyrolysis [22], pulse laser deposition [23], and sputtering [24,25]. Among them, sputtering deposition is particularly attractive due to its large area capability, uniform coating, and extensive usage in the semiconductor industry. In the past, highly conductive ITO thin films were obtained by sputtering through ITO sputter target or reactive sputtering of metallic (In–Sn) alloys in the O_2/Ar environment [26–28]. The reported results suggested that the resultant film properties are sensitive to deposition condition and post-annealing conditions [29]. As a result, the optimization strategy usually involves tuning the sputtered ITO film deposition in order to provide TCO films with high optical transmittance and low sheet resistance [30,31]. Clearly, this strategy is not suitable for the DSSCs process because during the TiO_2 sintering process, ITO tends to crack and

*Tel.: +886 97250 6900; fax: +886 73645589.
E-mail address: ianbu@hotmail.com

0272-8842/$ - see front matter © 2013 Elsevier Ltd and Techna Group S.r.l. All rights reserved.
http://dx.doi.org/10.1016/j.ceramint.2013.09.086

degrade its properties, which result in the increase of sheet resistance [32]. Consequently, in order to apply ITO to DSSCs, the sintering process-induced degradation has to be overcome. Although effects of annealing upon the non-optimized sputtered ITO have been investigated in previous studies [33–35], there are a limited number of studies on extending this knowledge to the fabrication of DSSCs [36]. Recently, Chen et al. [36] developed a two-step annealing process for commercially available ITO and achieved a power conversion efficiency of up to 6.7%. However, the current study proposes a different method that only applies a one-step annealing process in the air to the cost-effective, in-house manufactured ITO glass substrates. This alternative synthesized strategy enables the successful incorporation of ITO into DSSCs. It involves the deposition of non-optimized, opaque ITO thin film; followed by a simple annealing process on a hotplate that transforms the ITO thin films from opaque into optically transparent TCO and simultaneously performing the TiO_2 sintering process. It should be emphasized that the proposed strategy recovers non-stoichiometric ITO films, rather than repairing damaged films by the additional N_2 vacuum annealing process. It is shown that the proposed method is high-throughput and compatible with the current DSSCs fabrication process.

2. Experimental

Soda lime glass substrates were cleaned by acetone, methanol and D.I water under ultrasonic agitation. ITO films were then coated on the pre-cleaned substrates by DC magnetron sputtering using an ITO target (purity = 99.99%; diameter = 2 in.; thickness = 1 cm; In_2O_3:SnO_2 = 90:10 wt%) without external heating. The sputtering chambers were pumped down to 1×10^{-6} mbarr by a turbo pump. Then 10 sccm of argon gas was introduced into the sputter chamber via mass flow controller. Prior to the deposition, the sputter target was cleaned by Ar plasma with D.C. power set at 200 W for 30 min. During the cleaning process, the substrates were isolated from the plasma by a mechanical shutter.

For the actual sputtering deposition, the pressure and the DC power were maintained at 5×10^{-3} mbarr and100 W, respectively. The film thickness was controlled by deposition time. ITO glasses for the annealing experiment were heated in the air for 10 min on a hotplate set at 450 °C.

The photoanodes of dye sensitized solar cells were fabricated through a paste mixture of 0.3 g TiO_2 powder (P25, Degussa), 5 ml glacial acetic acid, and 1 ml Triton X-100 by using an agate mortar. The TiO_2 paste was then spread on the sputtered ITO glasses through a square mask (0.25 cm^2) by the doctor blade process and sintered at 450 °C on a hotplate for 1 h in order to evaporate the solvents. The final thickness of the TiO_2 film was around 15 μm. Prior to the device assembly, the photoanodes were immersed in 0.3 mM N719 dye in dry ethanol/acetonitrile mixture (1:1 in v/v) for one day. In order to fabricate the counter electrode, another piece of ITO glass was coated with a sputter layer of Pt with thickness of around 80 nm. Two small holes were drilled from the Pt coated ITO glass for electrolyte injection.

DSSCs solar cells were assembled by hot pressing a piece of Suryn sheet between the Pt glass and TiO_2 coated ITO glass.

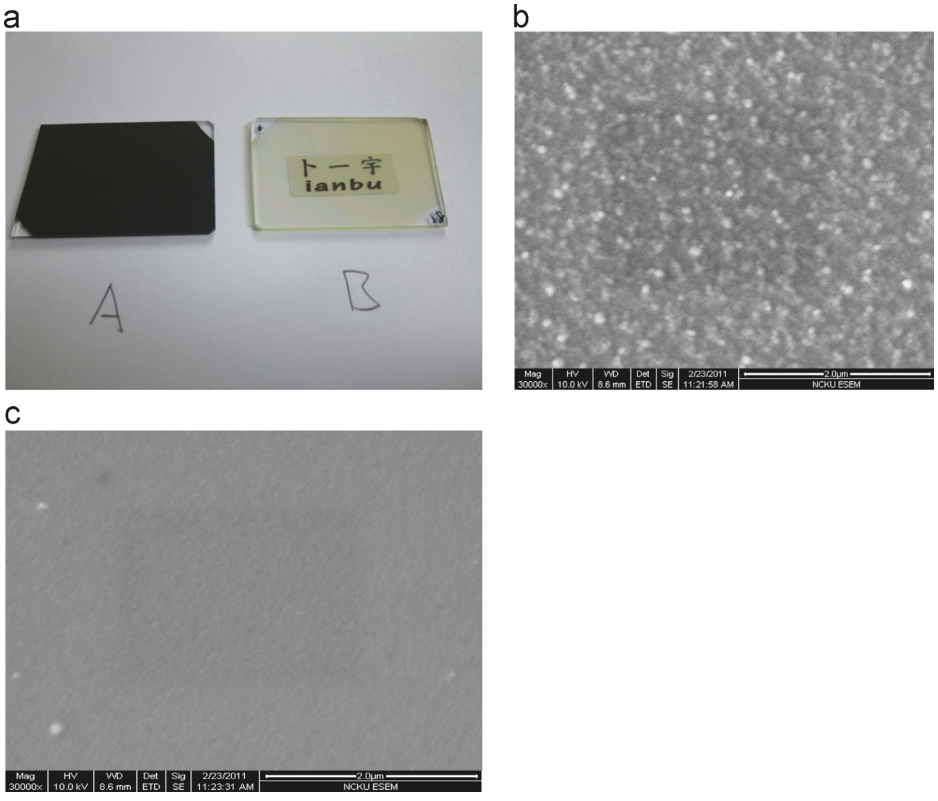

Fig. 1. (a) Photographic images of the as-deposited (A) and annealed sample (B), (b) SEM image of sample (A) and (c) SEM image of sample (B).

It was followed by the injection of electrolyte comprising lithium iodide (0.5 M), iodine (0.05 M), 4-tert-butylpyridine (0.5 M), and 1-methyl-3-propylimidazolium iodide (0.6 M) in 3-methoxypropionitrile. Finally, the pre-drilled holes were sealed by smaller pieces of Suryn sheets.

The film's morphology of sputter deposited ITO samples was obtained by using an FEI Quanta 400F Environmental Scanning electron microscope (SEM). A Siemens D5000 X-Ray diffractometer, which uses CuKα radiation, was adopted to assess the orientation and crystal structure of the ITO thin films. The sheet resistance was measured by a four-point probe measurement system. Transparency measurements were obtained through Jasco UV–vis spectroscopy, sweeping over the wavelength in the range of 200–1800 nm. *J–V* characteristics were measured by a PC controlled digital source meter (Keithley) illuminated by a solar simulator (Science tech).

3. Results and discussions

Fig. 1(a) shows the photograph of the as-deposited ITO glass (sample A) and films annealed at 450 °C (sample B), respectively. Clearly, sample A is opaque and the annealing process has induced a remarkable change in the ITO optical transmittance. It is well known that the optoelectronic properties of the ITO deposited in the sputter chamber are sensitive to deposition power, gas selection, gas flow rate and pressure. Consequently, under the optimized condition, it is possible to produce highly transparent ITO films in our laboratory. By controlling the power and gas flow pressure, it was possible to produce opaque ITO thin films, as presented in the left-hand side photograph of Fig. 1(a). Whilst the dark ITO thin film is unsuitable for transparent conductive oxide applications, it is a good base substrate for further DSSCs fabrication process. The effect of annealing on the ITO glass is shown in the right-hand side photograph of Fig. 1(a). It is interesting to observe that the appearance of ITO thin film has transformed from opaque to transparent after just a short period of annealing at 450 °C, which corresponds to the most commonly used annealing temperature for DSSCs fabrication. In order for us to understand the origin of transparency improvement, the samples' morphology is obtained by an FEI Quanta 400F Environmental Scanning electron microscope (SEM). Fig. 1(b) and (c) shows the SEM images of the as-deposited ITO thin film without and with annealing, respectively. Evidently, the annealing process has caused significant discrepancies between the surface morphology of the ITO film. Fig. 1(b) shows that the as-deposited ITO samples possess high surface roughness with grains of around 100–200 nm in diameter. In contrast, the annealed ITO thin film is smooth, without visible protrusions. Consequently, it can be concluded that the increased surface roughness of the ITO film must have enhanced light absorption due to increased scattering[37].

Fig. 2(a) shows the XRD patterns of the as-deposited and annealed ITO thin film. Clearly, the as-deposited ITO thin film possesses broad peaks that correspond to an amorphous-phase rich structure with non-stochiometric composition. Before the annealing process, due to the amorphous-phase of ITO, its XRD pattern shows a second diffusion hump that is close to $2\theta \approx 33^{\circ}$. Broad peaks of ITO have also been detected at (211), (222), (400), (411), (432), (431), (440), and (622) orientations. As suggested by the broadening of the XRD peaks in Fig. 2(a), the as-deposited samples contain significant amorphous phases that consist of defects. These defects include oxygen vacancies and grain boundaries within the film. However, the annealing process can effectively remove these defects through heat-induced restructuring and incorporation of oxygen into vacancy sites. It is interesting to note that the annealing process has sharpened these peaks. Evidently, this observation indicates the enhancement in crystallinity. Although it has been reported that the (400) diffraction intensity increases with film thickness [43,44], such a preference is absent in the present study. This result confirms that no change in the preferred crystal orientation has occurred during the annealing process. Further evidence can be found from Fig. 2(b), which shows the effect of annealing on the XRD peaks of the ITO film. No obvious differences in the XRD patterns have been observed within the range of film thickness considered in this study.

One of the key parameters of TCO is its optical transmittance. Fig. 3(a) shows the transmittance spectra of the annealed ITO

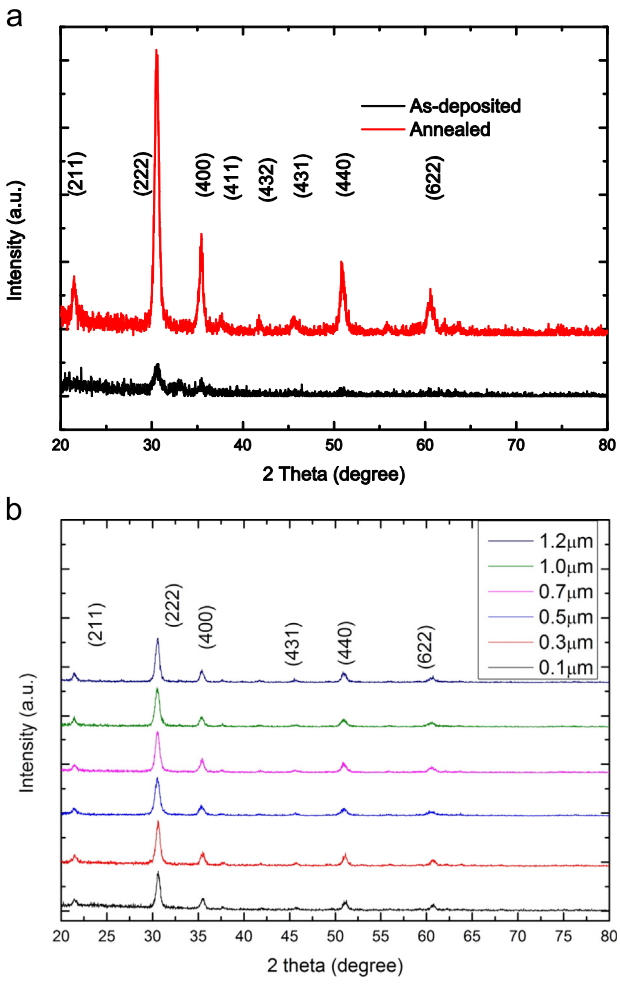

Fig. 2. XRD patterns of the sputtered ITO thin films (a) before and after annealing process and (b) of different thickness.

films with thickness ranging from 100 nm to 1.2 um. It is observed that, except when the film thickness equals 300 nm, the transmittance of the annealed ITO films decreases with the increase in film thickness. Furthermore, the transmittance near the absorption edge decreases with increasing film thickness. This tendency can be attributed to the higher probability of optical scattering that arises from longer optical paths, increased absorption, as well as Bragg reflection minima and maxima arising from different combinations of wavelength and thickness.

Fig. 3(b) shows the extracted optical transmittance versus film thickness at wavelength of 500 nm. Clearly, there is a critical thickness, with which the annealing process can work effectively. When the thickness exceeds 1 μm, the annealing process can only revert to 30% in optical transmittance. In general, commercially available ITO coated glass is around 250 nm in thickness and exhibits 88% optical transmittance at 500 nm. Consequently, our proposed annealing process is capable of recovering the optical transmittance that is comparable to commercially available ITO glass. It is also interesting to note that, as the thickness increases, the absorption edge of the annealed film tends to shift toward longer wavelengths. This phenomenon is often attributed to Burstein–Moss (BM) effect, which is closely related to the carrier concentration [45].

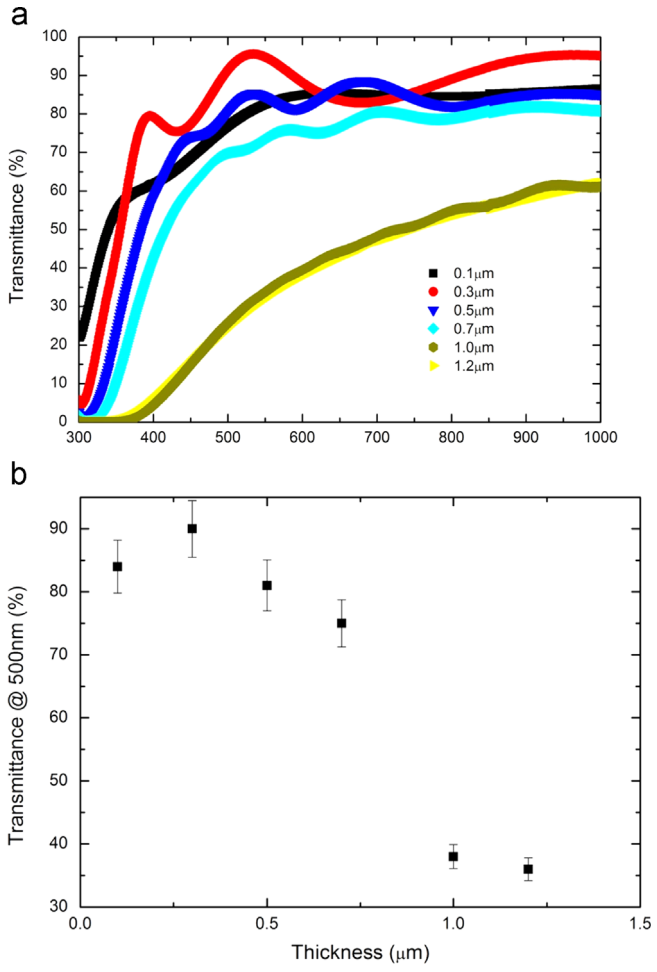

Fig. 3. (a) Optical transmittance of the annealed ITO thin film as function of film thickness and (b) extracted transmittance at wavelength 500 nm.

Eq. 1 shows its relationship

$$(\Delta E_g)_{\mathrm{BM}} = \left(\frac{h^2}{8m_{vc}^*}\right)\left(\frac{3n}{\pi}\right)^{2/3} \quad (1)$$

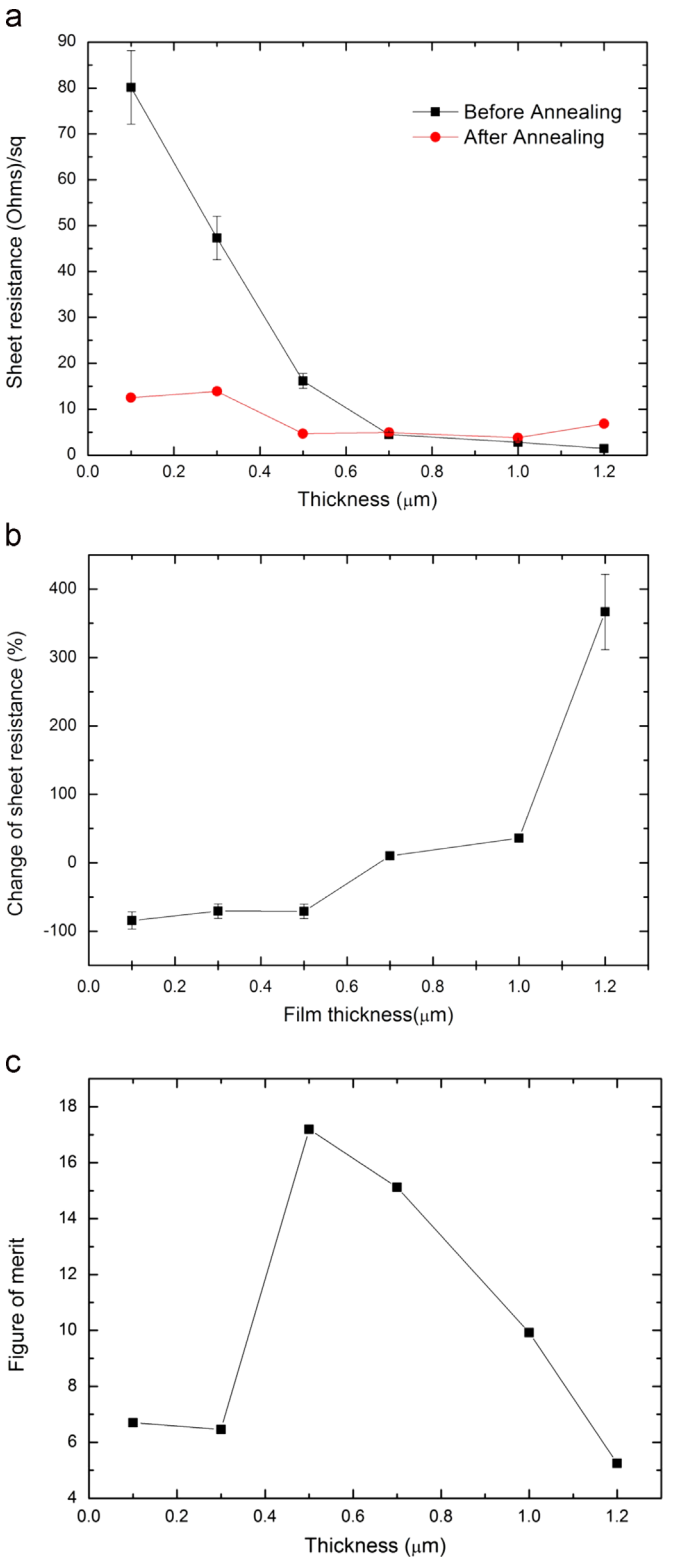

Fig. 4. (a) Variation of ITO film thickness with sheet resistance, (b) corresponding change in sheet resistance and (c) figure of merit transmittance at 500 nm: sheet resistance.

where ΔE_g is the band gap widening; m_{vc}^* is the conduction band effective mass; h is the Plank constant and n is the carrier concentration. Clearly, as the carrier concentration increases, the BM effect becomes significant and the band gap increases. As a result, the absorption edge shifts into the shorter wavelength region, which means that more energy is required to excite the carrier from valence to conduction band. The same rationale can also explain the shift of absorption edge to longer wavelengths due to the decrease in carrier concentration. This result is in good agreement with the previous study [46]. For ITO films

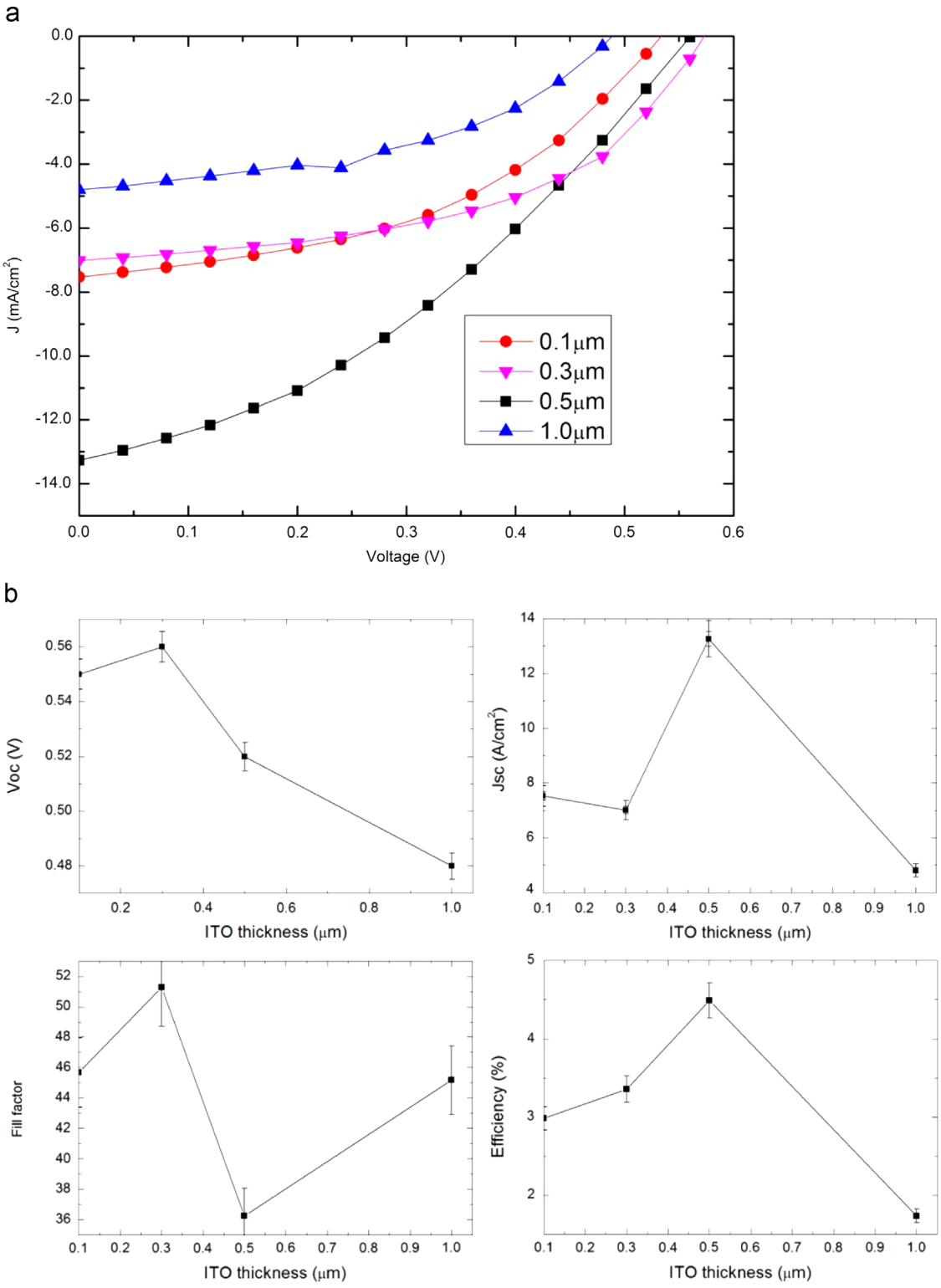

Fig. 5. (a) *J*–*V* characteristics of the fabricated DSSCs using ITO of different thickness and (b) extracted V_{oc}, J_{sc}, fill factor and power conversion efficiency from the fabricated device

deposited at room temperature, a decrease in free carrier concentration has been observed in thicker films due to the higher concentration of impurity states in the ITO films.

Fig. 4(a) shows the variation in sheet resistance, before and after annealing, with respect to the ITO thickness. Prior to the annealing process the sheet resistance of the ITO film with 100 nm thickness is approximately 80 Ω/sq. As the film thickness increases to about 300 nm, the resistance reduces by almost 50% to around 47 Ω /sq. This tendency continues until the thickness reaches 1.2 μm, the maximum thickness considered by this study. The presented results are in good agreement with the previous study [47] that attributes the difference in sheet resistivity to the initial amorphous film growth, which affects the thinner films. Fig. 4(b) shows the variation in sheet resistance as ITO film undergoes the annealing process. It is evident that the annealing process has caused thinner samples to have the most significant changes. However, as the thickness exceeds 500 nm, the annealing process actually increases the sheet resistances. This observation can be explained by the fact that, during the initial growth stage, the deposited ITO film is predominantly amorphous and possesses higher sheet resistance. Consequently, thinner ITO films will benefit most from the thermal re-crystallization during the annealing process. However, because thicker films contain more crystalline phases, they fail to fully benefit from the annealing process. The resulted higher sheet resistance in the annealed films (thicker than 500 nm) is probably due to the micro-crack formation in ITO [32]. Figure of merit for a transparent conductor can be defined by extracting the ratio of transmittance (at 500 nm): sheet resistivity, which is plotted in Fig. 4(c). Clearly, the ITO thin films with 0.5 μm in thickness possess the optimal combination of high optical transmittance and low sheet resistance.

In order to demonstrate the feasibility of the proposed method, DSSCs are constructed with ITO. Fig. 5 (a) gives the *J–V* curve of the DSSCs prepared with annealed ITO of different thicknesses. Fig. 5(b) shows the relationship between the thickness and open circuit voltage, short circuit current, fill factor and power conversion efficiency. Our result suggests a decrease in (open circuit voltage) V_{oc} when compared with DSSCs fabricated by using FTO. In general, the V_{oc} extracted from the DSSCs fabricated using FTO in our laboratory is around 0.68 V. However, the maximum V_{oc} observed from those with ITO is 0.58 V. The observed decrease is in good agreement with the previous study [48], in which a similar decrease in V_{oc} of DSSCs fabricated using ITO as the substrate is reported. It is well know that V_{oc} is very sensitive to the interface between conductive oxide and metal oxide. Therefore, the inherent decrease in V_{oc} as a function of ITO film thickness is probably due to the discrepancies in optical and structural properties of ITO deposited at different thickness.

The correlation between the fill factor (FF) and sheet resistance is plotted in Fig. 5(b) Generally, the FF in DSSCs can be affected by four factors: (1) the charge-transfer process at the counter electrode; (2) the carrier transported by ions within the electrolyte; (3) the thickness of the electrolyte layer; and (4) the sheet resistance of the TCO substrates. As the current study focuses upon the thickness of ITO, the sheet resistance of TCO substrates is most likely the cause for the observed tendency. On the other hand, the short circuit current density (J_{sc}) and power conversion efficiency (η) mirror closely to the extracted figure of merit plotted in Fig. 4(c). The maximum J_{sc} and η are observed when a 0.5 μm thickness ITO film is used as the substrate.

There is a trade-off in DSSCs between the sheet resistance of the TCO and its optical transmittance. Whilst the use of thicker TCOs can significantly reduce the sheet resistance, it will also result in a decrease in transmittance. It is expected that the optimum value for sheet resistance is around 10 Ω/sq with a transmittance of more than 80% in the visible spectral region. In fact, both parameters will affect the eventual power conversion efficiency of the fabricated device. The DSSCs device that produces the highest η (4.48%) has been fabricated by using ITO with 500 nm in thickness. Owing to the decrease in both the V_{oc} and short circuit current, further increase in the film thickness results in a decrease in η. This study indicates that the sheet resistance of thicker ITO thin films (with thickness greater than 500 nm) is not sensitive to further increase the film thickness. Consequently, the decrease in solar cell performance can be attributed to the opaque nature of thicker ITO films with transmittance below 40% at wavelength of 500 nm, which leads to insufficient incoming light for electron generation.

4. Conclusion

This study proposes a new strategy to utilize ITO thin films in DSSCs. Unlike the conventional TiO_2 nanoparticle sintering process for optimizing ITO films, the proposed process uses an amorphous-phase rich ITO film as the starting material. As a result, this process can maximize the benefits of the annealing process by thermally restructure to produce a highly transparent film with low sheet resistance. A critical thickness is identified for the annealing process. DSSCs of this study have achieved a maximum η of up to 4.48%.

References

[1] B. O'Regan, M. Grfitzeli, A low-cost, high-efficiency solar cell based on dye-sensitized, Nature 353 (1991) 24.
[2] I.Y. Bu, Sol–gel deposition of fluorine-doped tin oxide glasses for dye sensitized solar cells, Ceramics International (2013).
[3] H.-G. Bang, J.-K. Chung, R.-Y. Jung, S.-Y. Park, Effect of acetic acid in TiO < sub > 2 < /sub > paste on the performance of dye-sensitized solar cells, Ceramics International 38 (2012) S511–S515.
[4] Y. Wang, E. Chen, H. Lai, B. Lu, Z. Hu, X. Qin, W. Shi, G. Du, Enhanced light scattering and photovoltaic performance for dye-sensitized solar cells by embedding submicron SiO < sub > 2 < /sub > / TiO < sub > 2 < /sub > core/shell particles in photoanode, Ceramics International 39 (5) (2013) 5407–5413.
[5] S.-S. Lin, Effect of substrate temperature on the properties of TiO < sub > 2 < /sub > nanoceramic films, Ceramics International 38 (3) (2012) 2461–2466.
[6] T. Kawashima, T. Ezure, K. Okada, H. Matsui, K. Goto, N. Tanabe, FTO/ITO double-layered transparent conductive oxide for dye-sensitized solar cells, Journal of Photochemistry and Photobiology A: Chemistry 164 (1) (2004) 199–202.

[7] M. Dürr, A. Schmid, M. Obermaier, S. Rosselli, A. Yasuda, G. Nelles, Low-temperature fabrication of dye-sensitized solar cells by transfer of composite porous layers, Nature Materials 4 (8) (2005) 607–611.
[8] S. Ito, T.N. Murakami, P. Comte, P. Liska, C. Grätzel, M.K. Nazeeruddin, M. Grätzel, Fabrication of thin film dye sensitized solar cells with solar to electric power conversion efficiency over 10%, Thin Solid Films 516 (14) (2008) 4613–4619.
[9] F. Pichot, J.R. Pitts, B.A. Gregg, Low-temperature sintering of TiO_2 colloids: application to flexible dye-sensitized solar cells, Langmuir 16 (13) (2000) 5626–5630.
[10] L. Grinis, S. Kotlyar, S. Rühle, J. Grinblat, A. Zaban, Conformal nano-sized inorganic coatings on mesoporous tio2 films for low-temperature dye-sensitized solar cell fabrication, Advanced Functional Materials 20 (2) (2010) 282–288.
[11] R.G. Gordon, Criteria for choosing transparent conductors, MRS Bulletin 25 (8) (2000) 52–57.
[12] M.Y. Yen, C.Y. Yen, S.H. Liao, M.C. Hsiao, C.C. Weng, Y.F. Lin, C.C. M. Ma, M.C. Tsai, A. Su, K.K. Ho, A novel carbon-based nanocomposite plate as a counter electrode for dye-sensitized solar cells, Composites Science and Technology 69 (13) (2009) 2193–2197.
[13] J. Hotovy, J. Hüpkes, W. Böttler, E. Marins, L. Spiess, T. Kups, V. Smirnov, I. Hotovy, J. Kováč, Sputtered ITO for application in thin-film silicon solar cells: relationship between structural and electrical properties, Applied Surface Science 269 (2012) 81–87.
[14] S.H. Park, A. Roy, S. Beaupré, S. Cho, N. Coates, J.S. Moon, D. Moses, M. Leclerc, K. Lee, A.J. Heeger, Bulk heterojunction solar cells with internal quantum efficiency approaching 100 percent, Nature Photonics 3 (5) (2009) 297–302.
[15] T. Kim, S. Kim, S. Yang, J. Son, K. Lee, Y. Hong, K. Shim, J. Yang, K. Lim, S. Bae, GaN-based light-emitting diode with textured indium tin oxide transparent layer coated with Al_2O_3 powder, Applied Physics Letters 94 (16) (2009) (161107-161107-161103).
[16] C. O'Dwyer, M. Szachowicz, G. Visimberga, V. Lavayen, S. Newcomb, C.M.S. Torres, Bottom-up growth of fully transparent contact layers of indium tin oxide nanowires for light-emitting devices, Nature Nanotechnology 4 (4) (2009) 239–244.
[17] S. Wakeham, M. Thwaites, B. Holton, C. Tsakonas, W. Cranton, D. Koutsogeorgis, R. Ranson, Low temperature remote plasma sputtering of indium tin oxide for flexible display applications, Thin Solid Films 518 (4) (2009) 1355–1358.
[18] H. Wu, L. Hu, T. Carney, Z. Ruan, D. Kong, Z. Yu, Y. Yao, J.J. Cha, J. Zhu, S. Fan, Low reflectivity and high flexibility of tin-doped indium oxide nanofiber transparent electrodes, Journal of the American Chemical Society 133 (1) (2011) 27–29.
[19] Y.J. Jeong, S. Woo, Y. Kim, S.J. Jeong, Y.S. Han, D.K. Lee, J.I.I. Ko, S.K. Jung, B.C. An, Effects of solvents on ITO cracks in ultrasonic cleaning of ITO-coated flexible substrates for polymer solar cells, Molecular Crystals and Liquid Crystals 551 (1) (2011) 212–220.
[20] G. Socol, M. Socol, N. Stefan, E. Axente, G. Popescu-Pelin, D. Craciun, L. Duta, C. Mihailescu, I. Mihailescu, A. Stanculescu, Pulsed laser deposition of transparent conductive oxide thin films on flexible substrates, Applied Surface Science (2012).
[21] M. Alam, D. Cameron, Optical and electrical properties of transparent conductive ITO thin films deposited by sol–gel process, Thin Solid Films 377 (2000) 455–459.
[22] M.A. Aouaj, R. Diaz, A. Belayachi, F. Rueda, M. Abd-Lefdil, Comparative study of ITO and FTO thin films grown by spray pyrolysis, Materials Research Bulletin 44 (7) (2009) 1458–1461.
[23] H. Ohta, M. Orita, M. Hirano, H. Tanji, H. Kawazoe, H. Hosono, Highly electrically conductive indium–tin-oxide thin films epitaxially grown on yttria-stabilized zirconia (100) by pulsed-laser deposition, Applied Physics Letters 76 (2000) 2740.
[24] S. Ishibashi, Y. Higuchi, Y. Ota, K. Nakamura, Low resistivity indium–tin oxide transparent conductive films. II. Effect of sputtering voltage on electrical property of films, Journal of Vacuum Science and Technology A: Vacuum, Surfaces, and Films 8 (3) (1990) 1403–1406.
[25] S. Ishibashi, Y. Higuchi, Y. Ota, K. Nakamura, Low resistivity indium–tin oxide transparent conductive films. I. Effect of introducing H2O gas or H2 gas during direct current magnetron sputtering, Journal of Vacuum Science & Technology A: Vacuum, Surfaces, and Films 8 (3) (1990) 1399–1402.
[26] R. Joshi, V. Singh, J. McClure, Characteristics of indium tin oxide films deposited by rf magnetron sputtering, Thin Solid Films 257 (1) (1995) 32–35.
[27] M. Grundmann, Transparent conductive oxide semiconductors, The Physics of Semiconductors, 511–515.
[28] B. Houng, A. Wang, Characterization of indium tin oxide films by RF-assisted DC magnetron sputtering, Applied Surface Science 258 (15) (2012) 5593–5598.
[29] T. Karasawa, Y. Miyata, Electrical and optical properties of indium tin oxide thin films deposited on unheated substrates by dc reactive sputtering, Thin Solid Films 223 (1) (1993) 135–139.
[30] K. Sreenivas, T. Sudersena Rao, A. Mansingh, S. Chandra, Preparation and characterization of rf sputtered indium tin oxide films, Journal of Applied Physics 57 (2) (1985) 384–392.
[31] S.K. Park, J.I. Han, W.K. Kim, M.G. Kwak, Deposition of indium–tin-oxide films on polymer substrates for application in plastic-based flat panel displays, Thin Solid Films 397 (1) (2001) 49–55.
[32] M. Boehme, C. Charton, Properties of ITO on PET film in dependence on the coating conditions and thermal processing, Surface and Coatings Technology 200 (1) (2005) 932–935.
[33] C.-H. Yang, S.-C. Lee, S.-C. Chen, T.-C. Lin, The effect of annealing treatment on microstructure and properties of indium tin oxides films, Materials Science and Engineering: B 129 (1) (2006) 154–160.
[34] C. Guillén, J. Herrero, Influence of oxygen in the deposition and annealing atmosphere on the characteristics of ITO thin films prepared by sputtering at room temperature, Vacuum 80 (6) (2006) 615–620.
[35] G. Gonçalves, E. Elangovan, P. Barquinha, L. Pereira, R. Martins, E. Fortunato, Influence of post-annealing temperature on the properties exhibited by ITO, IZO and GZO thin films, Thin Solid Films 515 (24) (2007) 8562–8566.
[36] C.-M. Chen, Y.-C. Hsu, S.-J. Cherng, Effects of annealing conditions on the properties of TiO < sub > 2 < /sub > /ITO-based photoanode and the photovoltaic performance of dye-sensitized solar cells, Journal of Alloys and Compounds 509 (3) (2011) 872–877.
[37] G. Liu, J.B. Kerr, S. Johnson, Dark spot formation relative to ITO surface roughness for polyfluorene devices, Synthetic Metals 144 (1) (2004) 1–6.
[43] H. Kim, J. Horwitz, G. Kushto, A. Pique, Z. Kafafi, C. Gilmore, D. Chrisey, Effect of film thickness on the properties of indium tin oxide thin films, Journal of Applied Physics 88 (10) (2000) 6021–6025.
[44] C. Guillen, J. Herrero, Influence of the film thickness on the structure, optical and electrical properties of ITO coatings deposited by sputtering at room temperature on glass and plastic substrates, Semiconductor Science and Technology 23 (7) (2008) 075002.
[45] N. Patel, B. Lashkari, Conducting transparent indium-tin oxide films by post-deposition annealing in different humidity environments, Journal of Materials Science 27 (11) (1992) 3026–3031.
[46] C. Nunes de Carvalho, A. Luis, G. Lavareda, E. Fortunato, A. Amaral, Effect of thickness on the properties of ITO thin films deposited by RF-PERTE on unheated, flexible, transparent substrates, Surface and Coatings Technology 151 (2002) 252–256.
[47] D.H. Kim, M.R. Park, H.J. Lee, G.H. Lee, Thickness dependence of electrical properties of ITO film deposited on a plastic substrate by RF magnetron sputtering, Applied Surface Science 253 (2) (2006) 409–411.
[48] C. Sima, C. Grigoriu, S. Antohe, Comparison of the dye-sensitized solar cells performances based on transparent conductive ITO and FTO, Thin Solid Films 519 (2) (2010) 595–597.